Optics Communications 390 (2017) 105–110

Contents lists available at ScienceDirect

Optics Communications

journal homepage: www.elsevier.com/locate/optcom

Adaptive optics system based on the Southwell geometry and Improvement on control stability

Liang Wang[a], Xudong Lin[a], Xinyue Liu[a,*], Peifeng Wei[a,b]

[a] Changchun Institute of Optics, Fine Mechanics and Physics, Chinese Academy of Sciences, Changchun 130033, China
[b] University of Chinese Academy of Sciences, Beijing 100049, China

ARTICLE INFO

Keywords:
Adaptive optics
Southwell geometry
Control stability improvement
Shack-Hartmann wavefront sensor
Deformable mirror

ABSTRACT

An adaptive optics (AO) system has advantages of avoiding waffle modes and ease to assemble, when the lenslets of the Shack-Hartmann wavefront sensor (SH-WFS) and the actuators of the deformable mirror (DM) are configured according to the Southwell geometry. However, an AO system which follows the Southwell geometry suffers from the calibration difficulty and from the poor control stability. In this paper, an AO system based on the Southwell configuration is built up and experimentally demonstrated. The calibration problem is solved by adopting a DM which has an appropriate inter-actuator coupling, so that the movement of an actuator can be measured by the neighboring lenslets. The control stability is evaluated by the error propagators, and then, the control stability can be improved by filtering out smaller singular values of the response matrix. It is also shown that a tradeoff between the bandwidth error and the fitting error of an AO system can be made according to the error propagator. Finally, the performance measurement experiments indicate the reasonable ranges for the number of reserved singular values of the response matrix and the integrator gain, i.e. from 81 to 89, and from 0.2 to 0.5, respectively.

1. Introduction

Adaptive optics (AO) is a useful technique to improve the resolution of optical systems. Traditionally, AO was used to compensate atmospheric turbulence in the real time [1]. Recently, AO has been applied to many new fields such as high resolution microscopy [2], laser communication [3], laser space-debris cleaning [4], laser fusion [5] and ocular aberration correction [6].

An AO system generally comprises a wavefront sensor (WFS), a wavefront corrector (WFC) and a controlling system. The Shack-Hartmann wavefront sensor (SH-WFS) is a common-used WFS and the deformable mirror (DM) is a typical WFC. For an AO system with the zonal wavefront correction strategy, the controlling gradient directly (CGD) algorithm [7] is often adopted. The core of the CGD algorithm is to minimize local slopes, and consequently, the actuator voltages are evaluated during an iteration of the wavefront correction. In fact, the explicit wavefront reconstruction process is not required, and the mapping from the wavefront reconstruction to DM face-sheet space is done implicitly. However, in an AO system, the positions of DM actuators can be defined where the wavefront are estimated in the implicit wavefront reconstruction. Three conventional configurations of SH-WFS subapertures and DM actuators are depicted in Fig. 1. The horizontal lines and vertical lines represent the x-slope and y-slope sampling positions, respectively, and the crosses indicate the positions of SH-WFS subapertures. The dots represent the positions of DM actuators. The Fried's configuration [8], as is shown in Fig. 1(a), is very common in AO systems, such as in references [9–11]. However, the AO system with this configuration is not sensitive to waffle mode [7] and the subaperture has to be aligned at the center of four actuators accurately. The Southwell's configuration [12], as is shown in Fig. 1(b), can avoid producing waffle mode [1] which cannot be detected by SH-WFS. Because the actuators are positioned within, rather than around the lenslets, the Southwell configuration is useful in the case when the fine alignment between the lenslets and the actuators is not possible, or possibly dynamic. Nevertheless, this configuration yields difficulty in calibration because the movement of one actuator cannot be measured by its corresponding lenslet [13]. Also, the Southwell's configuration, which renders one-lenslet-to-one-actuator correspondence, may produce a response matrix with a large condition number, and therefore, the stability of closed-loop wavefront correction is reduced [14]. Additionally, it is known that the Southwell geometry may transmit more noise into actuator commands, compared with the Fried geometry. In order to overcome the disadvantages of the Fried's and the Southwell's configuration, a new kind of configuration with high-

* Corresponding author.
E-mail address: sirliuxy@hotmail.com (X. Liu).

http://dx.doi.org/10.1016/j.optcom.2016.12.076
Received 28 October 2016; Received in revised form 26 December 2016; Accepted 28 December 2016
Available online 05 January 2017
0030-4018/

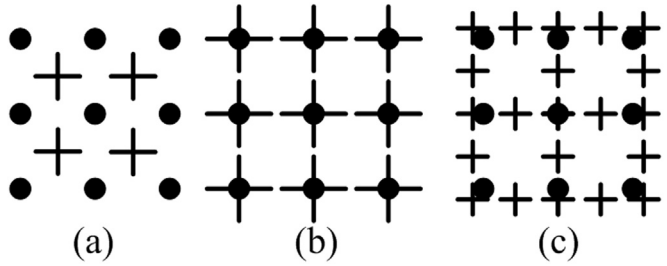

Fig. 1. Three configurations of SH-WFS subapertures and DM actuators.

density samples of slopes, as is illustrated in Fig. 1(c), was proposed and applied to the AO system [15]. This configuration increases the number of subapertures to avoid the waffle mode and increase the control stability. However, the target is achieved by sacrificing the illumination level of a single subaperture so that more light intensity is required. As a result, this configuration is not very suitable for observing dim astronomical objects.

In this paper, the authors build up an experimental AO system based on the Southwell geometry and try to overcome the disadvantages of the Southwell's configuration when it is applied to AO systems. Although many researchers have focused on this configuration in the field of wavefront reconstruction [16,17], the Southwell geometry is less popular in AO systems, than the Fried's geometry. In order to cope with the calibration difficulty, a DM with an appropriate coupling between neighboring actuators is developed, so that the movement of one actuator can be sensed by the neighboring subapertures. With respect to the low control stability, a method of filtering out small singular values of the response matrix is proposed and the control stability is evaluated by using the error propagator. And finally, the performance of the AO system is measured.

2. The experimental AO system

The experimental AO system built up in this paper is depicted in Fig. 2. The white light source and the interferometer are interchangeable, and the mirror M1 and the turbulence simulator (TS) are removable. A tip/tilt mirror (TM) is used to correct low-order aberrations of tip/tilt. This experimental AO system can work in three conditions. a) When calibrating the AO system, the white light source is moved in, whereas the interferometer, TS and M1 are removed. b) When correcting static aberrations, the white light source is moved in, and the TS is removed. First, the interferometer and M1 are removed temporarily, and a closed-loop wavefront correction begins. Then, the wavefront correction stops and the voltages of the actuators hold. Finally, the interferometer and M1 are moved back and the residual aberrations are measured, so as to estimate the performance of correcting static aberrations. c) When correcting dynamic aberrations, the white light source and TS are moved in, whereas both the interferometer and M1 are removed. Then, a closed-loop wavefront correction is carried out, and the Strehl ratio (SR) is computed according to the images obtained from the imaging camera so as to estimate the performance of correcting dynamic aberrations. The

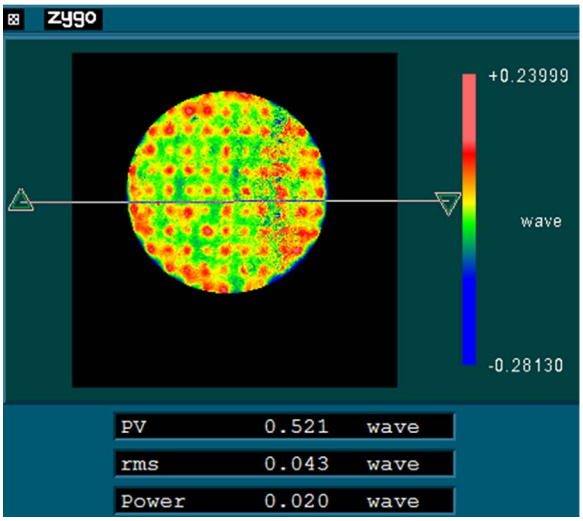

Fig. 3. The surface of the DM after flattening (The wavelength of the Zygo interferometer is 632.8 nm).

dimensions of the AO system are as follows, h_1=2880 mm and d_1=73 mm. The TS can move along the optical axis to simulate different Fried's coherent length r_0, which will be discussed in the Section 4.

In this system, both the 97-element DM and the SH are developed by Electro-Optical Detection Department of CIOMP. The inter-actuator coupling of the DM is about 20%. In order to test the precision of the DM, the DM is flattened by using the Zygo interferometer according to an iteration method [18]. Fig. 3 shows the surface of the DM after flattening, which is measured by the interferometer. The root mean square (RMS) and peak to valley (PV) is 0.043 wave (approximately λ/20, λ=632.8 nm) and 0.521 wave, respectively. The SH has 97 valid subapertures, the configuration of the SH and the DM follows the Southwell geometry, as is shown in Fig. 4. The small squares denote actuators of DM, the big squares denote subapertures of SH, and the number indicates the index of the subaperture. It is worth noting that some subapertures on the edge of the pupil are not included in the calculation of wavefront sensing. This is because the illumination level on these subapertures is very low, which will result in a low SNR and impair the control stability eventually.

3. Control stability improvement and evaluation

The CGD algorithm adopts the following equation to describe the response of an AO system,

$$\mathbf{s} = \mathbf{A}\mathbf{x}, \tag{1}$$

where **s** denotes the spot shifts of subapertures (in pixels), **x** denotes the normalized voltages of actuators, and **A** denotes the response matrix. Here, **s** is a vector of dimension $2m$, **x** is a vector of dimension n and **A** is a $2m \times n$ matrix, where m and n denote the subaperture number and the actuator number, respectively. For this AO system, both m and n equal to 97. The response matrix **A** can be obtained from a calibration process [13]. A response matrix of the experimental 97-

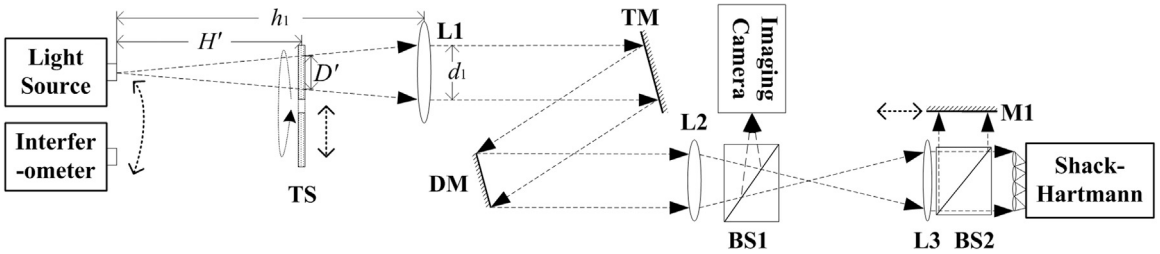

Fig. 2. The layout of the experimental AO system.

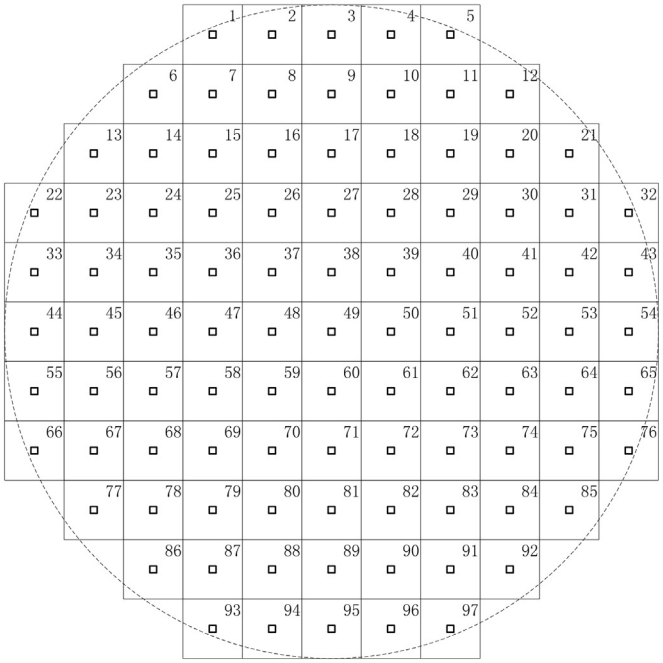

Fig. 4. The configuration of DM actuators and SH subapertures.

element AO system is measured. Fig. 5(a) shows the influence vector of the central actuator, i.e. the first column of **A**. Fig. 5(b) displays the 2D representation of this influence vector. In Fig. 5(b), small squares represent the positions of the actuators, and small circles refer to the positions of measured centroids when a unit voltage is set on the central actuator. Obviously, both the x-slope and the y-slope of the corresponding subaperture, the 49-*th* values, are very small. However, the slopes of the neighboring subaperture are remarkable, such as the x-slopes of the 37-*th*, 39-*th*, 48-*th*, 50-*th*, 59-*th* and 61-*th* lenslets, and the y-slopes of the 37-*th*, 38-*th*, 39-*th*, 59-*th*, 60-*th* and 61-*th* lenslets, and other slopes are merely noise. The signal to noise ratio (SNR) of x-slopes and y-slopes are 119.88 and 93.86, respectively. The results show that for the Southwell geometry, the influence of an actuator can be measured by the neighboring lenslets when the DM has an appropriate coupling between neighboring actuators.

In order to correct the wavefront aberrations, the actuator commands should be determined. The control equation of the AO system is as follows,

$$\mathbf{x} = \mathbf{B}\mathbf{s}, \tag{2}$$

where **B** denotes the control matrix of dimensions $n \times 2m$. The control matrix can be determined by computing the Moore-Penrose pseudo-inverse of the response matrix **A**. The singular value decomposition (SVD) [19] is a common algorithm for calculating the pseudo-inverse $\mathbf{A}^{\dagger}$. Then, $\mathbf{A}^{\dagger}$ can be used as the control matrix **B** in the Eq. (2).

The Lyapunov stability theory is a useful tool for stability analysis. In order to evaluate the improvement on the control stability, the propagator error [20] is adopted to estimate the control stability. The iteration equation of the closed-loop control of a zonal AO system is as follows,

$$\mathbf{x}_{i+1} = k\mathbf{B}\mathbf{s}_{i+1} + \mathbf{F}\mathbf{x}_i, \tag{3}$$

where k denotes the integral gain, and the subscript i and $i+1$ represent the i-*th* frame and the (i+1)-*th* frame, respectively. The matrix **F** is defined as follows,

$$\mathbf{F} \equiv a_0\mathbf{I} - k\mathbf{B}\mathbf{A}, \tag{4}$$

where **I** is an identity matrix, and a_0 denotes the proportional gain which is approximately unity. Then, the error propagator g_n is defined as follows,

$$g_n = \frac{k^2}{N_a}\mathrm{tr}\{[\mathbf{I} - \mathbf{F}^{\mathrm{T}}\mathbf{F}]^{-1}\mathbf{B}\mathbf{B}^{\mathrm{T}}\}, \tag{5}$$

where N_a denotes the number of controlled actuators in the pupil, and tr represents the trace of a matrix. The higher the error propagator is, the poorer the control stability is. Dubra partially attributed the instability of the closed-loop control to the smaller singular values of the response matrix [14], because the noise in the system modes corresponding to the smaller singular values might produce larger actuator voltages as a result of the reciprocal relationship in the calculation procedure of the pseudo-inverse of the response matrix. Then, therefore, we compute the error propagators for different response matrices by modifying the above response matrix which is obtained from the experimental AO system. The modification is filtering out a varying number of the smallest singular values. Also, the integral gain is varied from 0.1 to 1.0, with a step of 0.1, which covers the range of the common integral gains for AO correction. The results are shown in Fig. 6. It is worth noting that the control stability can be improved by reducing the integral gain and reserving less singular values of the response matrix. However, the integral gain and the number of reserved singular values should not be reduced at the same time because reducing the integral gain will increase the bandwidth error whereas filtering out more singular values of the response matrix will increase the fitting error, which will deteriorate the performance of the AO system. Therefore, a tradeoff can be made between the bandwidth error and the fitting error by using the error propagator. For example, to ensure the control stability in the case when the bandwidth error dominates, the bandwidth error can be lowered by increasing the integral gain at the expense of filtering out more singular values.

4. Performance measurement of the AO system

To test the performance of the AO system when a certain number of smaller singular values of the response matrix are filtered out, two experiments are carried out.

In the first experiment, both the number of reserved singular values and the integrator gain are varying, and the performance of the AO system are evaluated according to the RMS of residual aberrations which is measured by SH-WFS, when the static aberrations are being corrected. The frame rate of SH-WFS is 500 fps, and therefore, the correction frequency is 500 Hz. Table 1 shows the 200-frame average of the RMS of residual aberrations, when a closed-loop AO correction is executed. In order to avoid the influence of the beginning several frames, the RMS values of the first 100 frames are not taken into account and the average is calculated according to the subsequent 200 frames. It is worth noting that the system performance is relatively better, when the number of reserved singular values is in the range from 81 to 89 (The 85-*th* singular value is about 20% of the maximum singular value). Also, it can be found that the valid value for the integrator gain ranges from 0.2 to 0.5.

In the second experiment, the performance of the AO system are evaluated by using the residual aberrations (for the static aberrations) and the Strehl ratio (for the dynamic aberrations), when the integrator gain and the number of reserved singular values are set to typical values, 0.1 and 84, respectively. The correction frequency is also 500 Hz.

(a) Correcting the static aberrations. The residual aberrations are measured by using the interferometer, after the AO system has corrected the static aberrations. The purpose of using the interferometer is that the spatial resolution of the interferometer is much higher than the SH-WFS. The result is depicted in Fig. 7. It is shown that RMS of the residual aberrations is 0.051 wave after correcting the static aberrations (approximately λ/20, λ=632.8 nm).

(b) Correcting dynamic aberrations. The performance of the AO system can be evaluated by using the Strehl ratio, when the dynamic

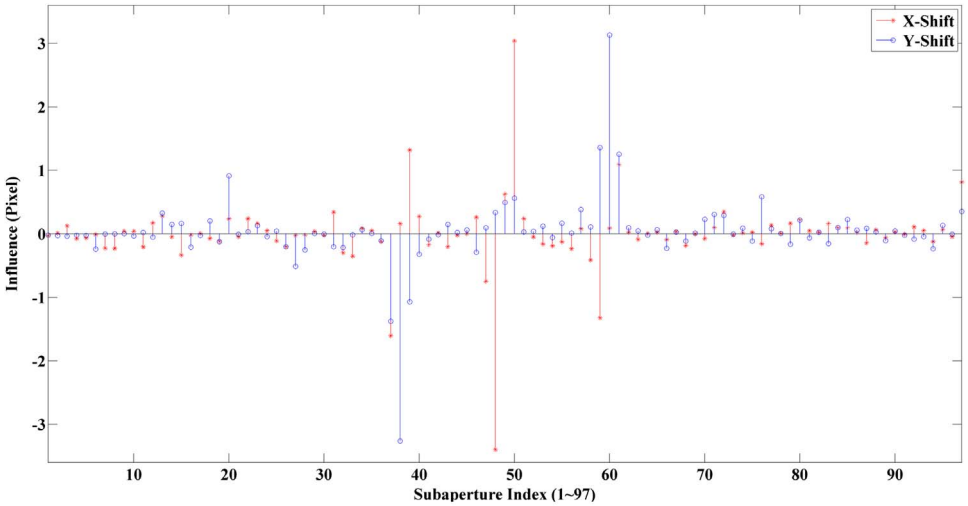

(a)1D representation of the influence vector

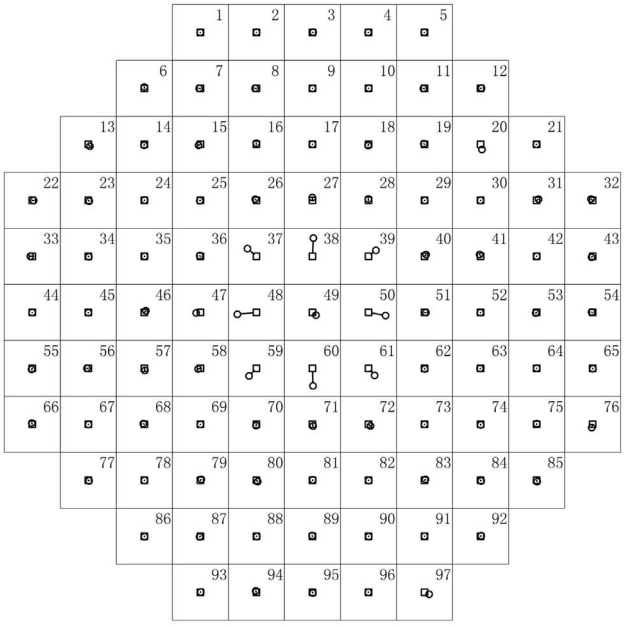

(b)2D representation of the influence vector

Fig. 5. The SH-WFS influence of the central actuator (a)1D representation of the influence vector (b)2D representation of the influence vector.

aberrations are corrected [21]. The dynamic aberrations are produced by the TS, and the Fried's coherent length r_0 and the Greenwood frequency f_G can be varied. The Fried's coherent length can be determined by

$$r_0 = \frac{r_0' D}{D'}, \tag{6}$$

where r_O' denotes the coherence length of the turbulence simulator (i.e. 0.6 mm@632.8 nm), D denotes the diameter of the pupil of the telescope in which the AO system is installed (i.e. 1.2 m), and D' denotes the valid diameter of the optical beam at the phase plate (see Fig. 2). Here, D' can be calculated by

$$D' = \frac{H' d_1}{h_1}, \tag{7}$$

where h_1 denotes the distance between the light source and lens L1, H' denotes the distance between the light source and the turbulence simulator, and d_1 denotes the valid diameter of the optical beam at L1. The Greenwood frequency f_G is determined by

$$f_G = 0.427 \frac{V}{r_0'}, \tag{8}$$

where V refers to the linear velocity of the turbulence simulator at the center of the optical beam. Therefore, r_0 can be modified by changing the distance between the turbulence simulator and the light source, and f_G can be adjusted by changing rotating rate of the turbulence simulator. Then, the performance measurement is conducted in the conditions when r_0 is set to 5 cm, 7 cm, 9 cm and 11 cm, respectively, and f_G is varied from 10 Hz to 100 Hz, with a step of 10 Hz. For each case, the wavefront correction is carried out, and 50 frames of images are saved from the imaging camera. Finally, an average Strehl ratio (SR) is computed according to the images from the imaging camera by using the method of Robert [22], so as to measure the performance of the AO system. The results are shown in Fig. 8. The results are comparable with the SR measured by Robert [22], though 13 lowest singular values of the response matrix are filtered out to improve the control stability.

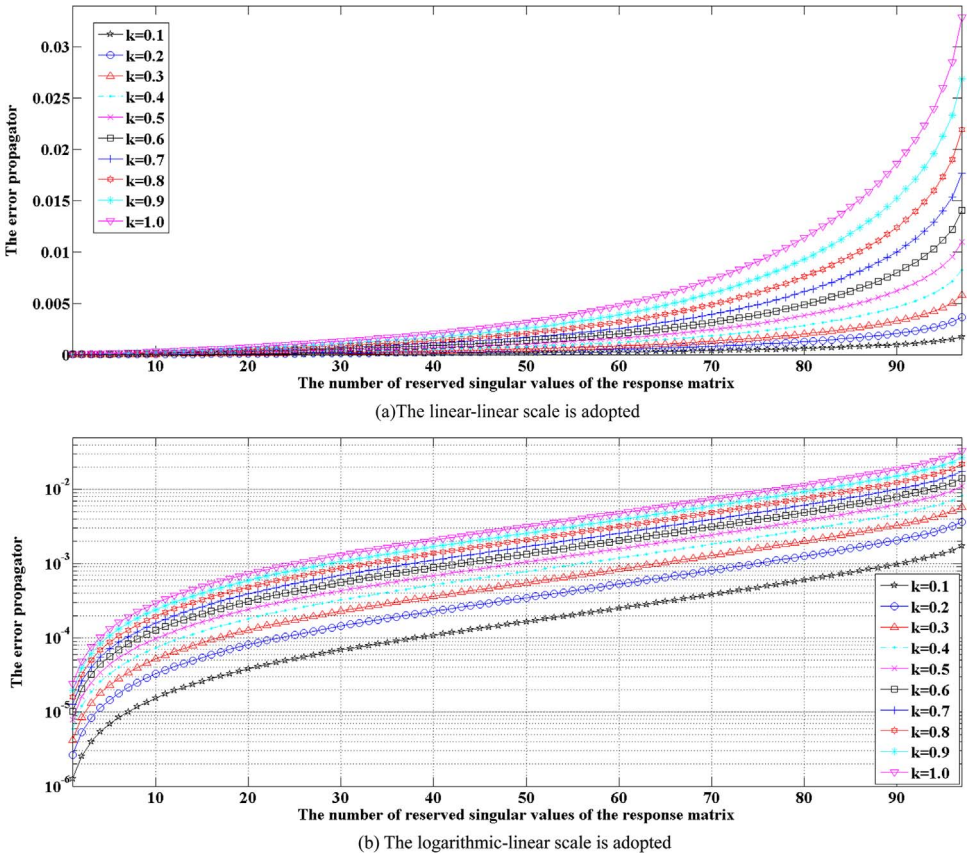

(a)The linear-linear scale is adopted

(b) The logarithmic-linear scale is adopted

Fig. 6. The error propagators versus varying number of reserved singular values of the response matrix (a)The linear-linear scale is adopted (b) The logarithmic-linear scale is adopted.

5. Conclusions

In conclusion, a 97-element AO system with the Southwell geometry has been constructed and experimentally demonstrated. The response matrix obtained from the calibration shows that the influence of the actuator can be measured by the slopes of the neighboring lenslets, when the DM has an appropriate inter-actuator coupling. The stability improvement method of filtering out several smaller singular values of the response matrix is validated by the error propagator. The error propagator can also be used to tradeoff the bandwidth error and the fitting error of an AO system. Finally, the results from the performance measurement experiments indicate that the reasonable values for the number of reserved singular values of the response matrix range from 81 to 89, and valid integrator gains range from 0.2 to 0.5, for this AO system. The performance of the AO system is also validated by experiments, when typical parameters are adopted, i.e. the number of filtered-out singular values is 13, and the integrator gain is 0.3.

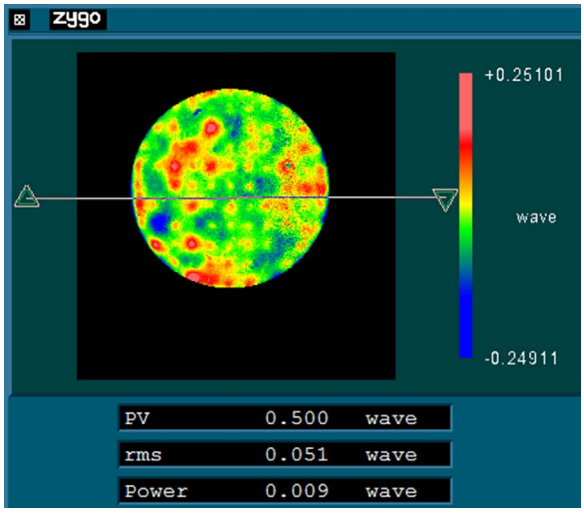

Fig. 7. The residual aberrations after correcting static aberrations. (The wavelength of the Zygo interferometer is 632.8 nm).

Acknowledgement

This work was supported by the National “863” Program of China

Table 1
200-frame average of RMS of the residual aberrations when the static aberrations are being corrected.

Number of reserved singular values	69	71	73	75	77	79	81	83	85	87	89	91	93	95
k=0.1	0.203	0.117	0.090	0.079	0.068	0.067	0.071	0.064	0.063	0.062	0.059	0.075	0.098	0.175
k=0.2	0.182	0.094	0.080	0.068	0.069	0.061	0.057	0.052	0.050	0.047	0.045	0.078	0.108	0.196
k=0.3	0.266	0.171	0.101	0.069	0.066	0.064	0.057	0.051	0.051	0.049	0.053	0.081	0.201	0.230
k=0.4	0.195	0.100	0.073	0.070	0.065	0.059	0.061	0.053	0.054	0.048	0.051	0.096	0.141	0.253
k=0.5	0.196	0.102	0.081	0.077	0.073	0.068	0.067	0.066	0.051	0.051	0.054	0.106	0.183	0.278
k=0.6	0.179	0.093	0.075	0.070	0.067	0.069	0.069	0.069	0.055	0.057	0.058	0.116	0.242	0.283

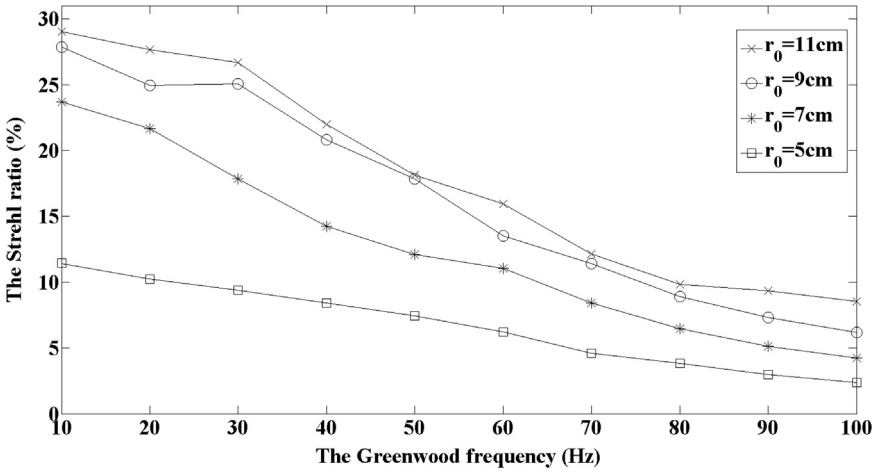

Fig. 8. The performance of the experimental AO system when correcting dynamic aberrations.

(No. 2014AAXXX1003X). The authors are grateful to the anonymous reviewers for their insightful comments, which improved this manuscript considerably.

References

[1] J.W. Hardy, Adaptive Optics for Astronomical Telescopes, Oxford University Press, New York, USA, 1998.
[2] M.J. Booth, Adaptive optical microscopy: the ongoing quest for a perfect image, Light: Sci. Appl. 3 (2014) e165.
[3] J. Huang, K. Deng, C. Liu, P. Zhang, D. Jiang, Z. Yao, Effectiveness of adaptive optics system in satellite-to-ground coherent optical communication, Opt. Express 22 (2014) 16000.
[4] A.M. Rubenchik, M.P. Fedoruk, S.K. Turitsyn, The effect of self-focusing on laser space-debris cleaning, Light: Sci. Appl. 3 (2014) e159.
[5] D. Homoelle, M.W. Bowers, T. Budge, C. Haynam, J. Heebner, M. Hermann, K. Jancaitis, J. Jarboe, K. LaFortune, Joseph Thaddeus Salmon, T. Schindler, M. Shaw, Measurement of the repeatability of the prompt flashlamp-induced wavefront aberration on beamlines at the National ignition facility, Appl. Opt. 50 (2011) 4382.
[6] D.X. Hammer, R.D. Ferguson, M. Mujat, A. Patel, E. Plumb, N. Iftimia, T.Y.P. Chui, J.D. Akula, A.B. Fulton, Multimodal adaptive optics retinal imager: design and performance, J. Opt. Soc. Am. A 29 (2012) 2598.
[7] W. Jiang, H. Li, Hartmann-Shack wavefront sensing and wavefront control algorithm, Proceedings of SPIE, 1271, 1990, pp. 82.
[8] D.L. Fried, Least square fitting a wave-front distortion estimate to an array of phase difference measurements, J. Opt. Soc. Am. 67 (1977) 370.
[9] J.M. Spinhirne, G.A. Ameer, Adaptive optics using the 3.5 m starfire optical range telescope, Proceedings of SPIE, 3126, 1997, pp. 257.
[10] C.R. Vogel, Q. Yang, Multigrid algorithm for least-squares wavefront reconstruction, Appl. Opt. 45 (2006) 705.
[11] E. Fedrigo, R. Muradore, D. Zilio, High performance adaptive optics system with fine tip/tilt control, Control Eng. Pract. 17 (2009) 122.
[12] W.H. Southwell, Wave-front estimation from wave-front slope measurements, J. Opt. Soc. Am. 70 (1980) 998.
[13] J. Porter, J.E. Lin, H.M. Queener, K. Thorn, A. Awwal, Adaptive Optics for Vision Science: principles, Practices, Design and Applications, Wiley-Interscience, 2005.
[14] A. Dubra, Wavefront sensor and wavefront corrector matching in adaptive optics, Opt. Express 15 (2007) 2762.
[15] H. Song, R. Fraanje, G. Schitter, G. Vdovin, M. Verhaegen, Controller design for a, Eur. J. Control 3 (2011) 290.
[16] G. Li, Y. Li, K. Liu, X. Ma, H. Wang, Improving wavefront reconstruction accuracy by using integration equations with higher-order truncation errors in the Southwell geometry, J. Opt. Soc. Am. 30 (2013) 1448.
[17] L. Huang, M. Idir, C. Zuo, K. Kaznatcheev, L. Zhou, A. Asundi, Shape reconstruction from gradient data in an arbitrarily-shaped aperture by iterative discrete cosine transforms in Southwell configuration, Opt. Laser Eng. 67 (2015) 176.
[18] A. Sivaramakrishnan, B.R. Oppenheimer, Deformable Mirror Calibration for Adaptive Optics Systems, Proceedings of SPIE, vol. 3353, 1998, pp. 910.
[19] X. Li, W. Jiang, Comparing between zonal reconstruction algorithms and modal reconstruction algorithms in adaptive optics system, Proceedings of SPIE, vol 4825, 2002, pp. 121.
[20] W.J. Wild, Lyapunov stability criteria for zonal adaptive-optics systems, Opt. Lett. 23 (1998) 570.
[21] L. Wang, T. Chen, X. Lin, P. Wei, X. Liu, J. Jia, Performance measurement of adaptive optics system based on Strehl ratio, The Journal of China Universities of Posts and Telecommunications, vol. 23, 2016, pp. 94.
[22] L.C. Roberts, C.R. Neyman, Characterization of the AEOS adaptive optics system, Publications of the Astronomical Society of the Pacific.